· Article · Advances in Polar Science
doi: 10.13679/j.advps.2018.3.00222 September 2018 Vol. 29 No. 3: 222-230

The study of ice shelf-ocean interaction—techniques and recent results

Keith W. NICHOLLS*

British Antarctic Survey, High Cross, Madingley Road, Cambridge CB3 0ET, UK

Received 14 June 2018; accepted 7 August 2018

Abstract Although the importance to global oceanography of ice shelf-ocean interactions has been recognized for many years, only more recently has its role in the control of ice flow from the interior, grounded ice sheet into the ocean been more clearly understood. The consequences for global sea level of increasing ice loss from the Antarctic and Greenland ice sheets has prompted rapidly growing research efforts in this area. Here we describe the different techniques commonly employed in the field study of ice shelf-ocean interactions. We focus on techniques used by the British Antarctic Survey, primarily on Filchner-Ronne Ice Shelf, and describe some recent results from instruments deployed both beneath the ice shelf and on its upper surface, which demonstrate variability at a broad range of time scales.

Keywords ice shelves, ice-ocean interaction, basal melt rates, hot-water drilling, polar oceanography

Citation: Nicholls K W. The study of ice shelf-ocean interaction—techniques and recent results. Adv Polar Sci, 2018, 29(3): 222-230, doi: 10.13679/j.advps.2018.3.00222

1 Introduction

Over the last decade the study of the interaction between ice shelves and the sea in which they float has gained much greater prominence. The main reasons have been the observation of the surface lowering of the West Antarctic Ice Sheet across neighboring glaciological catchments feeding ice shelves in the Amundsen Sea Embayment (Shepherd et al., 2004), attributed to regional oceanographic change, and theoretical advances underpinning the concepts of ice shelf buttressing, and the marine ice sheet instability (Schoof, 2007). The recognition that the uncertainty in predictions of sea level change are dominated by uncertainties in the future contribution from the West Antarctic Ice Sheet (Stocker et al., 2013) has increased the urgency of improving our understanding of the processes that lead to ice shelf change and the consequential changes in ice flux from ice sheet to ocean.

Numerical modelling is the methodology available to predict changes in sea level. But inherent limitations to the resolution of such models mean that many of the key processes will remain sub-grid scale for the foreseeable future, and need to be parameterized. Developing appropriate parameterizations requires a combination of finer-resolution modelling and detailed observations.

The importance of ice shelf-ocean interactions has also been acknowledged within the wider Southern Ocean oceanographic community. A workshop held in 2012 under the auspices of Southern Ocean Observing System (SOOS) resulted in a report outlining key observables required to progress understanding of the coupled sea ice-ocean-ice shelf system (Rintoul et al., 2014).

In this contribution we describe the observational techniques that have been used to provide data on ice shelf ocean interactions. The challenges are substantial: the presence of an ice shelf many hundreds of meters thick is a major barrier to direct observations of the ocean cavity beneath, and difficult sea-ice conditions routinely disrupt

* Corresponding author, E-mail: kwni@bas.ac.uk

attempts to reach the fronts of the ice shelves in order to carry out campaigns of ship-based oceanographic observations. Progress has nevertheless been made, and here we describe the techniques that have been used, and some examples of recent results.

We do not discuss satellite observations in detail. Although satellite-based observations are now yielding patterns of basal melting and freezing (Moholdt et al., 2014), rates of ice-shelf thinning (Paolo et al., 2015), and even time series of these parameters (Adusumilli et al., 2018), there remain questions about the reliability of the products over some ice shelves, particularly in the vicinity of grounding lines. One of the main concerns relate to the possibility of a time variation in the depth of penetration into the snow of radio waves from active radars, and the effect of spatial and temporal variability of surface accumulation rates and firn density. However, the broad patterns of melting and freezing seem robust between different methods used to process the datasets.

2 Ship-based observations

Although it can be difficult for ships to access an ice front, there is often a shore lead created by offshore winds. Therefore, if the ship can penetrate into the shorelead, it is then possible to undertake standard ship-based oceanographic observations, determine bathymetry at the seaward edge of the sub-ice shelf cavity, and deploy instruments moored to the sea floor.

Even with no data from within the cavity, ice front measurements can be used with an inverse modelling technique (Jenkins and Jacobs, 2008). In essence this is a black-box approach that compares the properties of waters leaving the cavity with those entering it. Typical measurements are temperature, salinity and dissolved oxygen, all of which are affected by melting or freezing at the ice shelf base. The idea is to invert the data and arrive at a best estimate of the basal melt rate integrated across the ice shelf. This approach has been used successfully for smaller ice shelves, but it assumes that the entire inflow and outflow have been captured by a conductivity-temperature-depth (CTD) section along the ice front. It can also be problematic if there is a significant seasonal variation, coupled with a cavity flushing time that is relatively long: it is important that the water that is measured exiting the cavity is responding directly to basal melting due to the water entering the cavity at the time of the CTD section.

One of the principal challenges faced when deploying moorings is the danger of iceberg damage. This means that the top of the mooring must be at a depth greater than the deepest-drafting icebergs likely to pass over the area, which has the effect of leaving the upper 200 to 300 m of water column unmonitored. Nevertheless, ice front moorings have been used to collect valuable datasets from several locations, including the Filchner-Ronne (Nicholls et al., 2003), Ross (Pillsbury and Jacobs, 1985), Amery (Herraiz-Borreguero et al., 2016) and Pine Island Glacier (Webber et al., 2017) ice shelves.

Ship platforms have been increasingly used for the deployment of autonomous underwater vehicles (AUVs) and gliders (Figure 1). The U.K. Autosub, developed by the National Oceanography Centre (NOC), has been successfully deployed beneath Fimbul Ice Shelf (Nicholls et al., 2006), Pine Island Glacier (Jenkins et al., 2010b), Ronne Ice Shelf and Filchner Ice Shelf. Gliders and profiling floats have used moored sound sources to navigate beneath Dotson Ice Shelf (Pers. Comm. from Pierre Dutrieux). Such vehicles give spatially more extensive snapshots of the conditions within the cavity, and some have a swath imaging capability to give detailed views of the ice base and sea floor morphology (Dutrieux et al., 2014).

Figure 1 Photograph of UK-NERC's Autosub 3 autonomous underwater vehicle about to be deployed in the Southern Ocean.

3 Direct access techniques (drilling)

Other than using AUVs, the only way of making direct measurements of conditions beneath an ice shelf is to make an access hole, usually using a pressurized hot-water drill (HWD) (Figure 2; Makinson and Anker, 2017).

3.1 Typical drilling methodology

Snow is first melted to provide a reservoir of water, usually stored in a flexible water container. The water is then pumped through oil-fueled heaters before being sent through a long hose to a nozzle. The nozzle is lowered slowly into the snow, at speeds that vary typically between 0.2 and 2 m per minute: the slower the nozzle descends, the wider the hole that is made.

The initial drilling consist of making a hole to a depth below the freeboard of the ice shelf, or the firn's pore close-off depth, whichever is deeper. A borehole pump is lowered to the bottom and the water pumped out to refill the water container. A parallel hole is then drilled, perhaps 0.7 m from the first, to the same depth. The nozzle is then left at

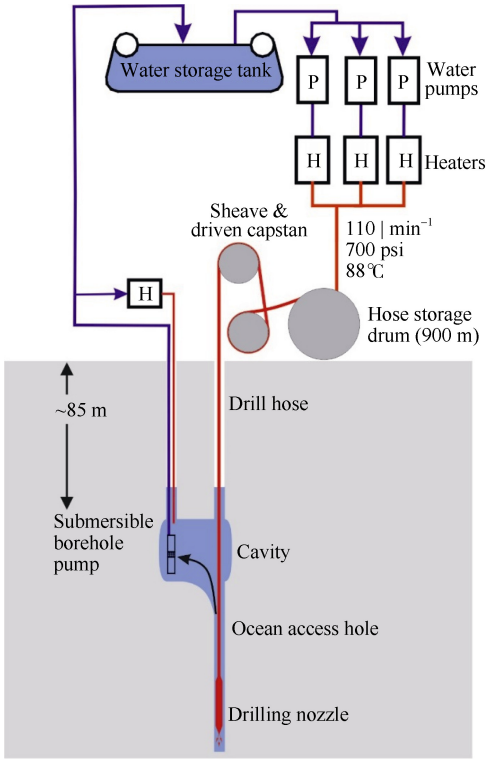

Figure 2 Schematic of the British Antarctic Survey ice shelf hot water drill. The depth of the cavity needs to be below sea level so that the submersible pump remains able to recover drilling water after the base of the ice shelf has been pierced.

that depth to connect the two holes, before the drill continues through the ice shelf with the drilling water being recovered by the borehole pump. Breakthrough is signaled by the water level in the borehole equilibrating at the ice shelf draft (corrected for freshwater).

3.2 Oceanographic observations via boreholes

Once the drill nozzle has been recovered, the access hole can be used until refreezing requires observations to be finished, or the hole is widened again with another pass of the drill. The observations typically made are a sequence of CTD profiles (Figure 3), and the permanent deployment of a set of instruments moored on a weighted mooring wire (Figure 4). The data are communicated to a data logger on the surface, and the individual instruments are either powered from the surface, via the mooring cable, or by their own batteries. Sensors in the moored instruments usually include temperature, and may also include conductivity, water velocity, pressure and dissolved oxygen.

Some recent deployments have utilized the distributed temperature sensor (DTS) technique, in which an optical fiber is interrogated by a spectrometer, and uses Raman scattering to determine the temperature profile along its length to an accuracy (with in situ calibration) of around 0.05℃ at a depth resolution of around 2 m (Stern et al., 2013; Tyler et al., 2013). This has proved effective for obtaining ice temperature profiles for glaciological

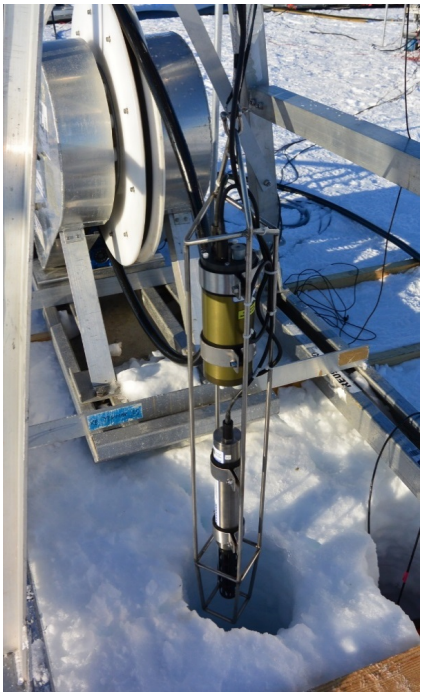

Figure 3 Photograph showing the CTD profiler (a SeaBird SBE49 "FastCat" with Power Data Interface Module), mounted in a frame and being deployed into the borehole.

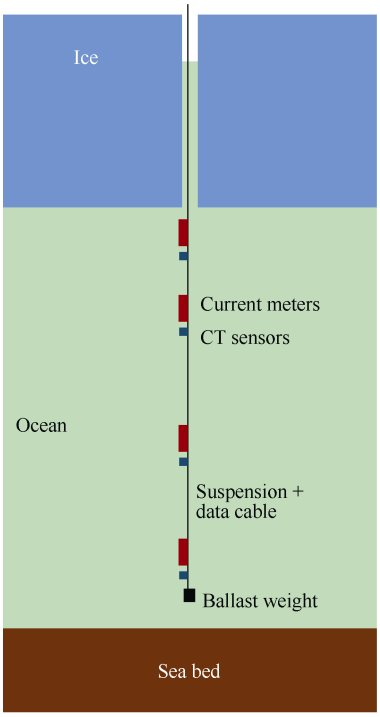

Figure 4 Schematic showing a typical mooring deployment through a hot-water drilled access hole.

purposes, and can be useful for relatively warm cavities that exhibit strong temperature signals. Powering a DTS spectrometer for long periods is challenging: there are very few long time series available from this technique. Another

method of obtaining time series of temperatures both through the ice and the water column is to use a thermistor cable—a multi-cored cable with thermistors embedded. Thermistor cables have the advantage of potentially high temperature resolution, are relatively cheap to construct, and do not require direct power.

Additional ways of exploiting a borehole have been to deploy slim, remotely operated vehicles (ROVs) that are capable of extending the spatial scale of the observations (Figure 5). Water samples have been recovered from beneath ice shelves using standard Niskin-like bottles, as well as specially-designed bottles for salinity and stable isotopes, and a water sampler designed to obtain samples for helium and neon concentrations.

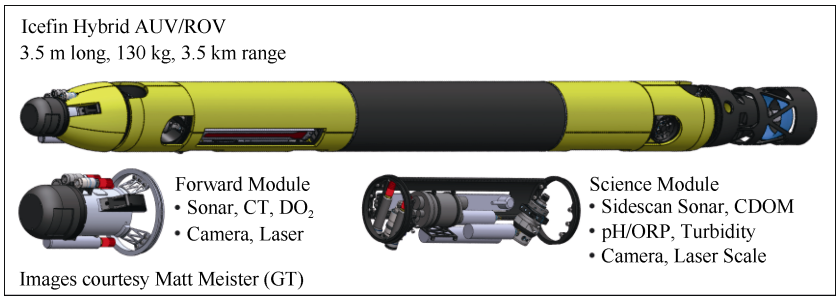

Figure 5 Schematic of the IceFin ROV, a vehicle capable of being deployed through a borehole (Schmidt et al., 2018).

Microstructure profilers have been successfully deployed through boreholes to give turbulent dissipation rates in the ice-ocean boundary layer (Venables et al., 2014). Turbulence instrument clusters (TICs) have also been successfully moored in the boundary layer (Stanton et al., 2013), and are now beginning to provide an improved description of the small-scale processes that mediate the heat, salt and momentum transport across this critical, upper part of the water column.

4 Measuring basal melt rates

A key measurement, both for the ice shelf and the underlying water column, is the ice shelf basal melt rate. The melt rate is primarily a function of the temperature in the upper water column, the stratification, and the strength of the water current. The temperature of the ice column itself plays only a weak role (Holland and Jenkins, 1999). The melt rate can therefore be regarded as fundamentally an oceanographic quantity, albeit one that is an essential part of determining the ice shelf's mass balance.

4.1 Indirect calculation of basal melt rates from glaciological observations

By conservation of ice mass, the rate of change of ice thickness can be approximated by

$$\frac{\mathrm{d}H}{\mathrm{d}t} + \underline{u}\cdot\underline{\nabla H} = H\underline{\nabla}\cdot\underline{u} - \frac{\left(\rho_0 w_0 - \rho_1 w_1\right)}{\rho}, \qquad (1)$$

where H is the ice thickness, $\underline{u}$ its horizontal velocity, w the vertical component of ice velocity and ρ the ice density. The suffixes "0" and "1" refer to the snow surface and ice base and the overbar indicates the vertical mean. If the ice thickness is known (from airborne radar echo-sounding, for example), and assumed to be constant in time, and the horizontal strain rates are measured using standard glaciological survey techniques, then the basal melt rate can be calculated, given the surface accumulation rate.

For some years the approach of using mass conservation was the most direct way of determining basal melt rates, although traditional survey methods were time intensive and impractical for a broad spatial coverage (Jenkins and Doake, 1991; Bishop and Walton, 1981).

The same approach is at the heart of deriving melt rates from satellite observations: the altimeter gives an estimate of the ice thickness by assuming the ice is freely floating, and there are various satellite-based approaches that can give the velocity field $\underline{u}$ (Moholdt et al., 2014). The only remaining variable is the surface accumulation rate. As satellite altimetry is able to determine $\mathrm{d}H/\mathrm{d}t$, the requirement for a steady ice thickness can be relaxed. Temporal and spatial variability in surface accumulation rate and the density of the upper firn remain problems for the interpretation of satellite data for some ice shelves where such variations are particularly strong.

4.2 Direct measurements of basal melt rate

In order to monitor ice shelf basal melt rates at timescales commensurate with the processes driving the melting, which are primarily oceanographic, other, more direct methods need to be employed. Where access holes through the ice shelf have been made, upward-looking sonars (ULS) can be installed, which give a direct measure of the melt rate (Nixdorf et al., 1994). This method has been successfully used to give melt rates at timescales down to weeks.

In the absence of a borehole, a radar technique can be used to monitor basal melt rates (Nicholls et al., 2015). With a ground-based radar to monitor the thinning of the ice shelf using a Lagrangian measurement (the radar moves with the ice flow), the left hand side of (1) is measured, and the melt rate can be calculated provided the ice strain rate (first term on the right hand side of (1)) can be deduced. As the ice column typically contains internal

reflecting horizons throughout its depth, the ice vertical strain rate (negative of the first term on the right hand side) can be calculated by measuring the relative displacement of those internal reflections. By using the internal reflections as a datum, the effects of surface accumulation are removed. The instrument developed to do this, the autonomous phase-sensitive radio echo-sounder (ApRES), is typically left in position for a year, making measurements every few hours (Figure 6). ApRES is able to monitor melt rates at timescales from interannual down to diurnal or even shorter.

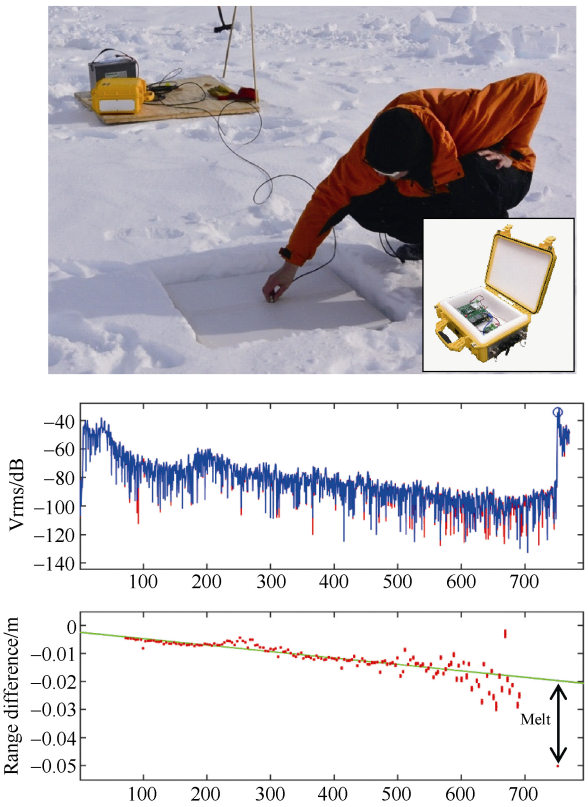

Figure 6 ApRES (inset photograph) being deployed. The main photograph shows a coaxial cable from the instrument being connected to one of the buried antennas. The graphs below show an example of the data acquired. Two measurements are being compared, separated by 10 d. Upper panel shows the two radar returns, with the bed visible at a depth of 770 m. Lower panel shows the difference in range to internal reflectors and the base, between the two measurements. The slope of the graph gives the vertical strain rate of the ice column, with the offset between a linear fit to those data and the displacement for the basal return giving the total basal melt during that 10-day period.

5 Case study from Ronne Ice Shelf

Here we describe some fieldwork that has recently been undertaken by the British Antarctic Survey to illustrate the types of datasets that can be obtained using some of the techniques discussed above.

5.1 Fieldwork

During the 2014–2015 field season, Site 5 on Ronne Ice Shelf was visited by a team from the British Antarctic Survey (Figure 7). In fact, three sites were occupied, sites 5a, 5b and 5c. The sites formed a triangle, with side lengths of around 6 km. The ice thickness across the sites ranged from 757 to 775 m, and the water column thickness from 354 to 400 m.

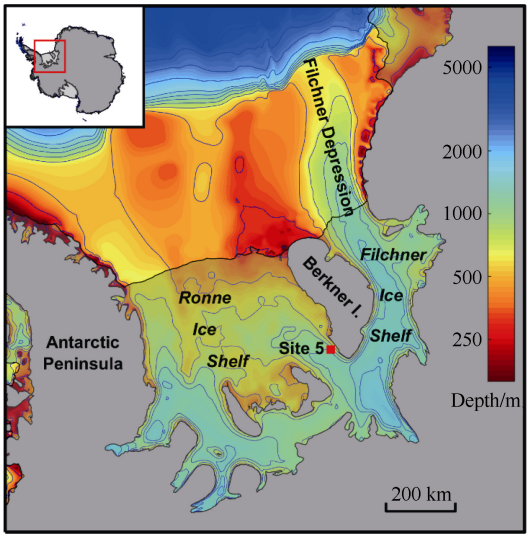

Figure 7 Map showing the location of Site 5 and the bathymetry of region (note non-linear color scale).

The specifications of the hot-water drill that was used are given in Figure 2. After drilling the access hole, a set of CTD profiles were obtained, and some sediment cores recovered. Different styles of moorings were deployed at each site.

A system built by Aanderaa was installed at Site 5a, with Seaguard instruments moored at five depths. Each instrument comprised an acoustic Doppler current meter, and temperature, conductivity and dissolved oxygen sensors. The instruments were powered from the topside controller-logger, with data stored locally and transmitted via Iridium datalink.

A thermistor cable manufactured by RBR Ltd. was deployed at Site 5b, with the downhole logger inductively coupled to the topside data logger using the armor jacket of a looped DTS system. In this way, the DTS system gave the temperature profile through the ice shelf, and the more sensitive thermistor cable gave the temperatures in the water column.

At Site 5c, two Nortek Aquadopps, five RBR CT instruments and two SeaBird CT Microcats were deployed, communicating to the topside logger using inductive modems.

At sites 5b and 5c the instruments and modems are powered by lithium thionyl chloride battery packs, with a nominal lifetime of around 10 years. As at Site 5a, the topside controllers stored data locally, and transmitted it via

Iridium data links.

An ApRES was run while the sites were occupied, and one was left running at each of the three sites through the following winter. An error during deployment caused the ApRES at Site 5a to fail. A full year of data was captured by the ApRES at Site 5c, and 9 months of data from Site 5b.

Except for the ApRES and the instruments at Site 5a, which were sampled at hourly intervals, all instruments were sampled every two hours.

5.2 CTD data and sediment cores

The mean absolute salinity and conservative temperature profiles for each site are shown in Figure 8. The entire water column below the ice base is below the surface freezing point, and has therefore either interacted with the ice base, or has mixed with water masses that have had such interaction. Comparison between the three sites needs to be done with care: as we show below, there is significant temporal variability in the area, and a week or more separate the dates at which the CTD profiles were obtained from each site.

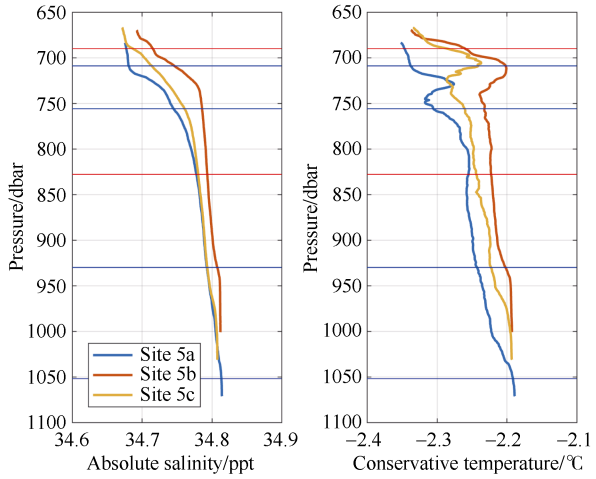

Figure 8 Profiles of absolute salinity and conservative temperature for the three sites (5a, 5b and 5c). The horizontal lines show the positions of conductivity and temperature (CT) sensors (blue) and CT sensor-current meter clusters (red) for Site 5c (The CTD profile for Site 5c does not reach the sea floor) .

Obtaining sediment cores from these sites proved difficult. We assume that the strong currents caused the corer to become inclined to the vertical before reaching the sea floor. Nevertheless, several sediment cores up to 50 cm in length were successfully recovered.

5.3 Mooring data from Site 5c

5.3.1 Eddies at Site 5

The first year of mooring data from the instruments at Site 5c, which were obtained from the beginning of 2015, is shown in Figure 9. The top panel shows that the temperatures exhibit a long-term variation that those future years of data (not shown) confirmed was seasonal, overlaid with significant interannual variability. There is a dominant short-term signal in these data that is interpreted as being due to the passage of warm-cored, anti-cyclonic eddies. The density of eddy activity is strongest when the current (shown, low-pass filtered, in Figure 9) is highest, although the strength of individual eddies appear strongest (measured by azimuthal velocity) when the eddy density is lowest. The cross-flow velocities from the two current meters shown in the third panel (see Figure 8 for the position of the moored instruments in the water column), indicate that the eddies appear to be intensified towards the ice base, although the mean flow velocities increase with depth in this part of the water column (Figure 9b). The data shown in Figures 9a and 9c have been band-pass filtered to remove low-frequency variations and variations at tidal frequencies and higher. What is particularly clear from this dataset is that the eddies themselves appear to play a significant role in bringing heat from the deeper water towards the ice base.

5.3.2 Source of the water at Site 5

When water interacts with an ice shelf base, melting results in the seawater giving up heat to provide the latent heat for melting, and taking up the fresh meltwater. The resulting changes in temperature and salinity are simply and linearly related, assuming that the heat conducted into the ice shelf to warm the ice to the melting point is small. On a T-S diagram, the result is that the properties of the water mass move along a straight line of gradient approximately 2.5℃ per 1‰ salinity. This means that from the T-S properties of a water parcel, it is possible to estimate the salinity of the source water for that parcel, if we know the source water's temperature.

Assuming that the source water is formed by sea-ice production, its temperature will be at or near the surface freezing point. With this assumption Figure 9d shows the variation in source salinity of the water measured about 25 m below the ice base, and a few meters above the sea floor. CTD profiles from ship-based observations along Ronne Ice Front show an approximately monotonic east-west increase in salinity. We therefore deduce that the waters of higher source salinity were derived from inflows further west. Thus the water from the deeper part of the water column likely originated from nearer the Antarctic Peninsula, and that from the upper water column came from the ice front nearer to Berkner Island.

5.3.3 Melt rate time series from ApRES

The melt rates measured from the ApRES deployed at Site 5c for the same period as the mooring data are shown in Figure 9e (black line). The data have again been low-pass filtered with a 2-day cutoff. The most striking feature is the strong variability in the melt rate. The mean value for the year is 1.25 $m \cdot a^{-1}$, yet, even after low-pass filtering, the melt signal varies from around 0.2 $m \cdot a^{-1}$ to a peak value of about 3.6 $m \cdot a^{-1}$.

Numerical models of sub-ice shelf circulation calculate oceanographic properties in the cavity beneath the ice shelf,

and they need to be able to calculate the rate of melting at the ice-shelf base that those conditions will drive. Various parameterizations have been used to diagnose ice shelf basal melt rates from modelled properties (Holland and Jenkins, 1999). They are usually driven by the temperature above the in situ freezing point, and possibly also the water speed, both taken from model nodes in the ocean boundary layer below the ice base. Using data from the moored instruments nearest the ice base, we can compare the results of parameterizations with observed melt rates. The cyan line in Figure 9e is a result of selecting one such parameterization, recommended by Jenkins et al. (2010a), and adjusting the drag coefficient at the ice base to obtain an optimal fit between the measured melt rate and that predicted by the parameterization.

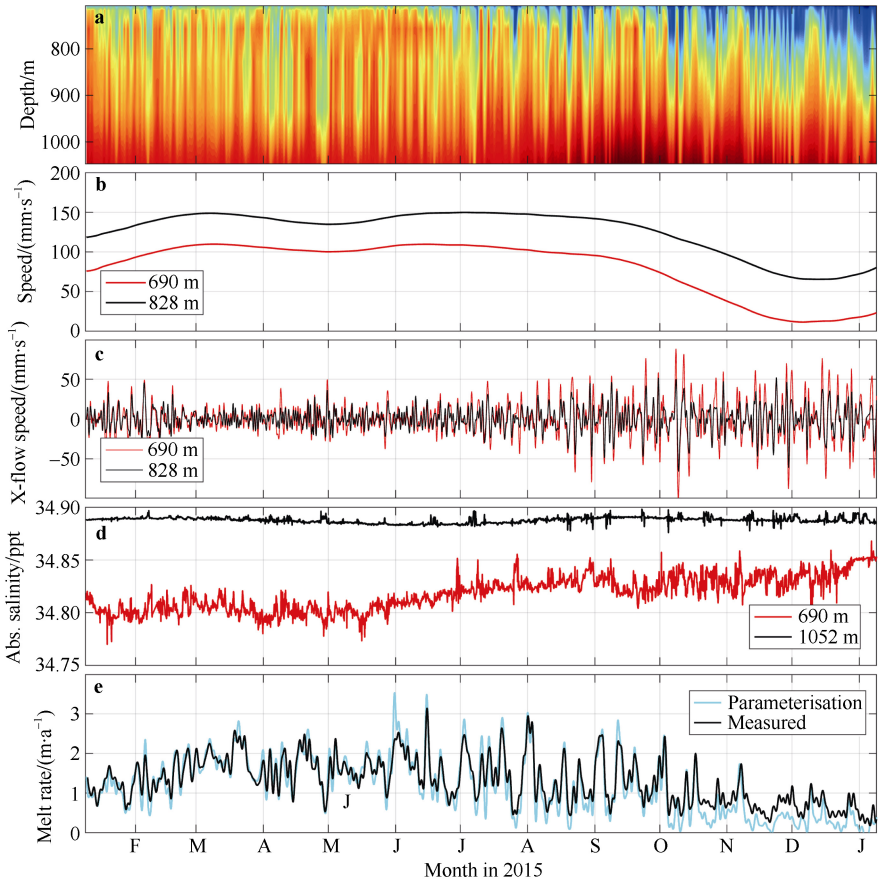

Figure 9 Some 12-month long datasets from the Site 5c mooring. **a**, Evolution of the temperature in the water column at Site 5c. **b**, Low-pass filtered, along-mean-flow water speeds at 690 and 828 m depth (see Figure 8 for the position of the instruments). **c**, Cross mean flow speed for the two current meters. Band-pass filtering is between 6 and 1.5 d to highlight eddy-like timescales of variability. **d**, Absolute salinity of source for waters at top and bottom of the water column, calculated assuming source water temperatures at the surface freezing point, and modification due purely to melting and freezing of ice at the ice shelf base. **e**, Basal melt rates from ApRES, after using a low pass filter at 2-day cut off. Also shown is the melt rate calculated using water temperature and speed from instruments 25 m below the ice base, with a parameterization recommended by Jenkins et al. (2010), but with tuned drag coefficient.

Overall, the measured and calculated melt rates are in good agreement, the only consistent and significant discrepancy arising towards the end of the record. Figure 8 shows that there were relatively strong vertical temperature gradients at the sites near the ice base (the top of the profile). The shallowest instruments moored at Site 5c were located deeper than originally planned, placing them in a strong part of the gradient (Figure 8). We assume this to be the root cause of the discrepancy. The under-prediction of the melt rate during the last few months of the record could be explained by a reduction in the temperature gradient in the upper few tens of meters of the water column. The optimization process mentioned above will have been appropriate for the bulk of the time series, in which the measured temperature was significantly greater than the temperature near the ice base because of the higher vertical temperature gradient. So if the temperature gradient in the upper water column reduces, the temperature measured by the instrument and used in the parameterization will reduce, but the temperature near the ice base will remain the same.

The variability in the melt rate in the 3–5 days band is a result of the warm-cored eddies passing the site, visible in the oceanographic records. Correlation between the melt rate time series from the ApRESs deployed at sites 5b and

5c, again show these features to be travelling at the speed of the mean flow.

The importance of the eddies for the overall melt rates observed at the site suggests that their absence from numerical models of sub-ice shelf oceanographic conditions, or their inadequate parameterization, will have a significant effect on modelled melt rates, for this site, at least. From Figure 9, it is clear that the warm cores occupy a significant portion of the water column, even over a time average, suggesting that they contribute substantially to the overall transport of heat and salt around the cavity.

6 Concluding remarks

The introduction of AUVs capable of spending significant periods of time beneath ice shelves is likely to provide a step change in our view of ice-ocean interactions. They remain expensive, and require significant infrastructure to deploy and operate (ships and possible insonification of the cavity), but they are likely to become a potent weapon in the researcher's arsenal of the future.

Glaciological approaches to studying the basal mass balance of ice shelves have been given a new lease of life with the use of satellite imagery and altimetry in place of traditional, ground-based survey methods. This technique still struggles with grounding zones and the confounding effects of variability in time and space of snow accumulation rates and surface conditions, but coarse time series of basal mass balance are now being produced.

The all-important times series of oceanographic observations from beneath ice shelves still rely on access holes created using hot-water drills. This is demanding on logistics, and time-consuming. However, it has the advantage of not requiring ship-access to the ice shelf, as it can usually be undertaken using aircraft-based logistics, and the data can usually be transmitted via a satellite link in pseudo-real time. As a result, the dataset is not lost if for some reason the site cannot be revisited.

The advent of recording, low-power, and highly-precise radars has opened up another approach to obtaining long records of ice shelf basal melt rates, with a temporal resolution capable of capturing the effect of processes operating at oceanic timescales. Such radars are relatively simple to deploy, with a low logistical burden, yet they can provide time series well-suited to testing and validating numerical models of sub-ice shelf processes.

Acknowledgments The author is grateful for the careful reading of the manuscript by two anonymous reviewers and for their suggestions and corrections.

References

Adusumilli S, Fricker H A, Siegfried M R, et al. 2018. Variable basal melt rates of Antarctic Peninsula ice shelves, 1994–2016. Geophys Res Lett, 45: 4086-4095, doi: 10.1002/2017GL076652.

Bishop J F, Walton J L W. 1981. Bottom melting under George VI Ice Shelf, Antarctica. J Glaciol, 27(97): 429-447.

Dutrieux P, Stewart C, Jenkins A, et al. 2014. Basal terraces on melting ice shelves. Geophys Res Lett, 41(15): 5506-5513, doi: 10.1002/2014gl060618.

Herraiz-Borreguero L, Church J A, Allison I, et al. 2016. Basal melt, seasonal water mass transformation, ocean current variability, and deep convection processes along the Amery Ice Shelf calving front, East Antarctica. J Geophys Res-Oceans, 121(7): 4946-4965.

Holland D M, Jenkins A. 1999. Modeling thermodynamic ice-ocean interactions at the base of an ice shelf. J Phys Oceanogr, 29(8): 1787-1800.

Jenkins A, Doake C S M. 1991. Ice-ocean interaction on Ronne Ice Shelf, Antarctica. J Geophys Res, 96(C1): 791-813, doi: 10.1029/90JC01952.

Jenkins A, Jacobs S. 2008. Circulation and melting beneath George VI Ice Shelf, Antarctica. J Geophys Res-Oceans, 113: C04013, doi: 10.1029/2007jc004449.

Jenkins A, Nicholls K W, Corr H F J. 2010a. Observation and parameterisation of ablation at the base of Ronne Ice Shelf, Antarctica. J Phys Oceanogr, 40: 2298-2312, doi: 10.1175/2010JPO4317.1.

Jenkins A, Dutrieux P, Jacobs S S, et al. 2010b. Observations beneath Pine Island Glacier in West Antarctica and implications for its retreat. Nat Geosci, 3(7): 468-472, doi: 10.1038/ngeo890.

Makinson K, Anker P G D. 2017. The BAS ice-shelf hot-water drill: design, methods and tools. Ann Glaciol, 55(68): 44-52, doi: 10.3189/2014AoG68A030.

Moholdt G, Padman L, Fricker H A. 2014. Basal mass budget of Ross and Filchner-Ronne ice shelves, Antarctica, derived from Lagrangian analysis of ICESat altimetry. J Geophys Res-Earth, 119(11): 2361-2380, doi: 10.1002/2014jf003171.

Nicholls K W, Padman L, Schröder M, et al. 2003. Water mass modification over the continental shelf north of Ronne Ice Shelf, Antarctica. J Geophys Res, 108: C8, doi: 10.1029/2002JC001713.

Nicholls K W, Abrahamsen E P, Buck J J H, et al. 2006. Measurements beneath an Antarctic ice shelf using an autonomous underwater vehicle. Geophys Res Lett, 33: L08612, doi: 10.1029/2006GL025998.

Nicholls K W, Corr H F J, Stewart C L, et al. 2015. A ground-based radar for measuring vertical strain rates and time-varying basal melt rates in ice sheets and shelves. J Glaciol, 61(230): 1079-1087, doi: 10.3189/2015JoG15J073.

Nixdorf U, Oerter H, Miller H. 1994. First access to the ocean beneath Ekstromisen, Antarctica by means of hot-water drilling. Ann Glaciol, 20: 110-114.

Paolo F S, Fricker H A, Padman L. 2015. Volume loss from Antarctic ice shelves is accelerating. Science, 348(6232): 327-331, doi: 10.1126/science.aaa0940.

Pillsbury R D, Jacobs S S. 1985. Preliminary observations from long-term current meter moorings near the Ross Ice Shelf, Antarctica. Oceanology of the Antarctic Continental Shelf, 43: 87-107.

Rintoul S, Van Wilk E, Wåhlin A, et al. 2014. Seeing below the ice: A strategy for observing the ocean beneath Antarctic sea ice and ice shelves. Report of the Southern Ocean Observing System. Tasmania.

Schmidt B E, Lawrence J D, Meister M R, et al. 2018. Under ice robotic exploration of the McMurdo Sound and Ross Ice Shelf//Ocean Worlds.

Proceedings of the conference held on 21-23 May, 2018 in Houston. Texas. doi: 2018LPICo2085.6051S.

Schoof C. 2007. Ice sheet grounding line dynamics: Steady states, stability, and hysteresis. J Geophys Res-Earth, 112: F03S28, doi: 10.1029/2006jf000664.

Shepherd A, Wingham D, Rignot E. 2004. Warm ocean is eroding West Antarctic Ice Sheet. Geophys Res Lett, 31(23): L23402, doi: 10.1029/2004GL021106.

Stanton T P, Shaw W J, Truffer M, et al. 2013. Channelized ice melting in the ocean boundary layer beneath Pine Island Glacier, Antarctica. Science, 341(6151): 1236-1239, doi: 10.1126/science.1239373.

Stern A A, Dinniman M S, Zagorodnov V, et al. 2013. Intrusion of warm surface water beneath the McMurdo Ice Shelf, Antarctica. J Geophys Res, 118: 7036-7048, doi: 10.1002/2013JC008842.

Stocker T, Qin D, Plattner G, et al. 2013. IPCC, 2013: Climate Change 2013: The Physical Science Basis. Contribution of Working Group I to the Fifth Assessment Report of the Intergovernmental Panel on Climate Change. UK: Cambridge University Press.

Tyler S W, Holland D W, Zagorodnov V, et al. 2013. Using distributed temperature sensors to monitor an Antarctic ice shelf and sub-ice-shelf cavity. J Glaciol, 59(215): 583-591, doi: 10.3189/2013JoG12J207.

Venables E, Nicholls K, Wolk F, et al. 2014. Measuring turbulent dissipation rates beneath an Antarctic ice shelf. Mar Technol Soc J, 48(5): 18-24.

Webber B G M, Heywood K J, Stevens D P, et al. 2017. Mechanisms driving variability in the ocean forcing of Pine Island Glacier. Nat Commun, 8: 14507, doi: 10.1038/ncomms14507.